

Article

Current Effect on the Performances of All-Solid-State Lithium-Ion Batteries—Peukert’s Law

A. S. Rudy ^{1,*}, A. M. Skundin ², A. A. Mironenko ¹ and V. V. Naumov ¹

¹ Department of Nanotechnology in Electronics, Physical Faculty, P.G. Demidov Yaroslavl State University, Sovetskaya St. 14, 150003 Yaroslavl, Russia; amironenko55@mail.ru (A.A.M.); vvnau@rambler.ru (V.V.N.)

² Frumkin Institute of Physical Chemistry and Electrochemistry, 119071 Moscow, Russia; office@phyche.ac.ru

* Correspondence: rudy@uniyar.ac.ru; Tel.: +7-(903)-826-58-54

Abstract: The results from measuring the capacity of thin-film solid-state lithium-ion batteries (SSLIBs) $Ti|Si@O@Al|LiPON|LiCoO_2|Ti$, $Ti|Si@O@Al|LiPON|Li_xV_2O_5|Ti$, and $Ti|LiPON|LiCoO_2|Ti$ at different charge currents are reported. It is shown that the dependence of the capacity on the current density $Q(j)$ follows Peukert’s law, which is characterized by a low value of Peukert’s exponents in the region of low currents and a high value of the exponents in the region of high currents. Peukert’s exponent for the anode-free cell remains constant through the entire range of current density variation. A model for SSLIB capacity based on the balance of ion (diffusion and drift) and electron currents is proposed. The model predicts a $Q(j)$ dependence well approximating the experimental results and fitting Peukert’s law. The model allows a qualitative interpretation of the change in the Peukert exponent with increasing current density, based on the effect of the charge current saturation.

Keywords: all-solid-state lithium-ion batteries; Peukert’s law; battery model; Peukert’s exponent

1. Introduction



Citation: Rudy, A.S.; Skundin, A.M.; Mironenko, A.A.; Naumov, V.V. Current Effect on the Performances of All-Solid-State Lithium-Ion Batteries—Peukert’s Law. *Batteries* **2023**, *9*, 370. <https://doi.org/10.3390/batteries9070370>

Academic Editor: Mingtao Li

Received: 19 May 2023

Revised: 26 June 2023

Accepted: 6 July 2023

Published: 10 July 2023



Copyright: © 2023 by the authors. Licensee MDPI, Basel, Switzerland. This article is an open access article distributed under the terms and conditions of the Creative Commons Attribution (CC BY) license (<https://creativecommons.org/licenses/by/4.0/>).

Solid-state thin-film lithium-ion batteries (SSLIBs) are an important, and simultaneously very specific, type of rechargeable chemical power source [1–4]. In the last decade, simultaneously with the expansion of the scope of SSLIB application, a steady growth was observed in the number of studies aimed at increasing their capacity and stability. In most of the SSLIBs, a solid electrolyte lithium phosphorus oxynitride (LiPON) is used [5]. LiPON has a number of advantages over other solid-state electrolytes, such as manufacturability, relatively high conductivity, very low electron transfer number, and a wide potential window of ~5 V. In recent years, a class of quasi-solid aqueous electrolytes featuring an improved stability and Coulombic efficiency of the order of 99% has appeared [6]. Such materials are of interest in terms of their implication in ionoelectronics, mechanics and optics. The most widely used electrode materials for industrial batteries at the moment are carbon and lithium cobaltite. Research on silicon application as a negative electrode is not widely adopted, due to its instability as the anode material. Obtaining a stable electrode material based on silicon is possible only in the form of the $Si@O@Al$ nanocomposite, which nevertheless has a high specific capacity—from 1.000 to 3.000 $\mu A \cdot h/g$ (depending on the ratio of elements) [7].

Some types of SSLIBs, including thin-film structures $Ti|Si@O@Al|LiPON|LiCoO_2|Ti$ and $Ti|Si@O@Al|LiPON|Li_xV_2O_5|Ti$, were the objects of our recent studies [7,8]. SSLIB cells were tested at room temperature, under various charge–discharge rates. With an increase in the charging current, a reduction in the capacity was observed. In a number of cases, the capacity dependence on current was well described by Peukert’s law [9]:

$$Q = \frac{A}{I^\alpha} \quad (1)$$

where Q is the battery discharge capacity, I is the discharge current, A is an empirical constant, and α is Peukert's exponent. For most kinds of batteries, this parameter varies between 1.0 and 1.3 [10].

The applicability of Peukert's law to lithium-ion batteries has been debatable up to now, although there are certain references to the fact of they obey this law. It is noteworthy that Peukert's law, empirically drawn in 1897 and valid for a narrow range of currents and temperatures [11–13], remains in the spotlight to this day, since it is directly related to the actual problem of battery control. Unfortunately, the literature data on the applicability of Peukert's law to SSLIB are few and far between. A Peukert's exponent close to 0.8 was reported in [7]. Ref. [14] describes an SSLIB with $\alpha \approx 0.69$.

For batteries operating in extreme conditions, such as in vehicles, an adequate model is required that can predict the behavior of the battery in any circumstance [15]. To build and implement a battery control algorithm, a method for estimating the state of charge (SoC) is needed, since all parameters of the battery model depend on this factor. Plenty of works are devoted to this issue, a review of which can be found, e.g., in [16,17]. A number of approaches to estimating SoCs, for example, Ref. [18], are based on the calculation of ampere-hours, which requires an accurate determination of the Peukert's law parameters. Therefore, the number of studies devoted to modeling lithium-ion batteries and calculating the parameters of Peukert's equation continues to grow steadily.

As a rule, battery models that follow Peukert's law are phenomenological in nature, i.e., based on experimental regularities. In this paper, we consider a simplified battery model based on the equations for the balance of diffusion and drift flows of charge carriers in a stationary mode. As shown below, the current balance condition is a certain ratio of lithium ion concentrations at the anode and cathode, which decreases with increasing current density.

2. Experiment

The derivation below of the SSLIB model is based on the experimental charge-discharge regularities obtained for cells of different electrochemical systems. The test cells were manufactured by high-frequency magnetron sputtering [7] at the SCR-651 "Tetra" (Alcatel, France) system using mask technology. Technological parameters of functional layer deposition are given in Table 1. Table 2 contains the structural parameters of test cells. Titanium foil, 10 μm thick, or preliminarily oxidized silicon wafers with a silicon dioxide thickness of 0.8 μm were used as substrates. The electrode layers were deposited with due account for differences in cathode and anode densities, as well as in the thickness of their layers. Therefore, the change in potential of the negative electrode in the course of galvanostatic cycling was negligible. The last test cell (third row of Table 2) was performed in an anode-free configuration.

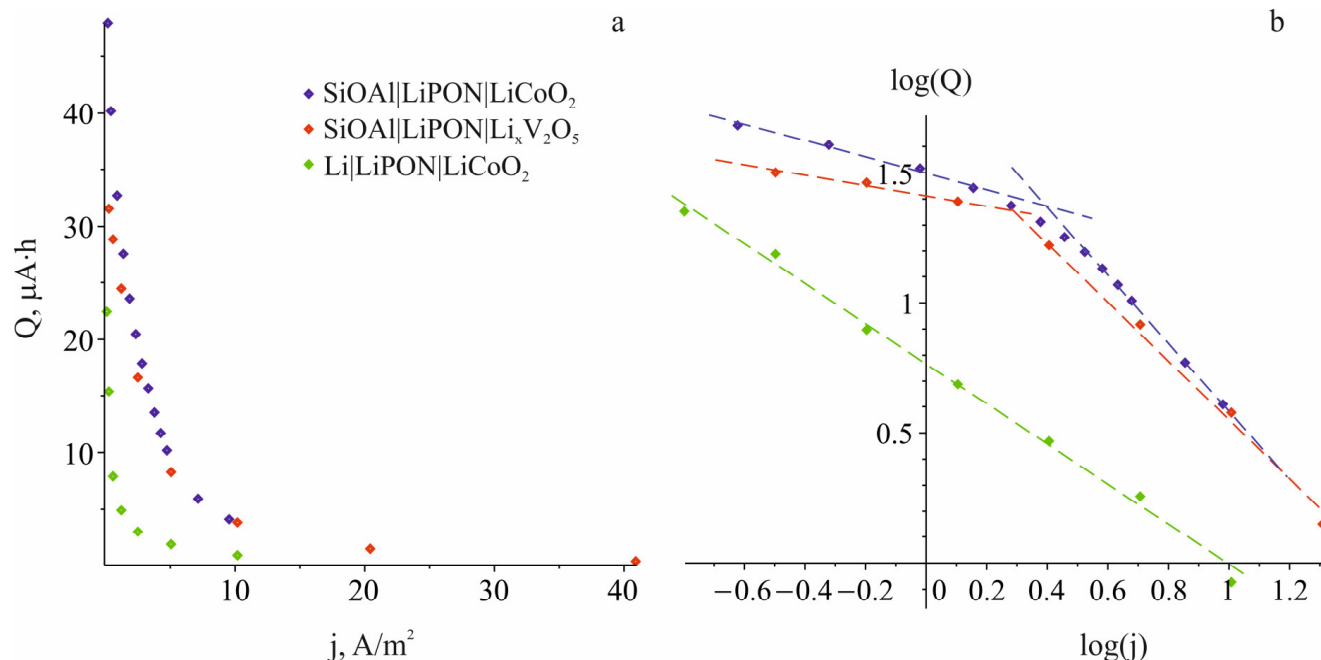
Table 1. Technological parameters for deposition of cells' functional layers by magnetron RF sputtering.

Layer	Target	Ar Flow, sccm	O ₂ Flow, sccm	N ₂ Flow, sccm	Pressure, Pa	Magnetron Power, W	Deposition Time, min
Si@O@Al	Alloy Si-Al (9:1)	200	0.6	-	1.75	600	6
LiPON	Li ₃ PO ₄	-	-	18.6	0.2	150	165
LiCoO ₂	LiCoO ₂	20	5	-	1	200	190
Li _x V ₂ O ₅	Li _x V ₂ O ₅	20	2	-	0.23	200	320
Down conductor	Ti	20	-	-	0.2	300	10

Table 2. Structural parameters of test cells.

Cell #	Parameters	Negative Electrode	Solid Electrolyte	Positive Electrode
1	Layer composition	Si@O@Al	LiPON	LiCoO ₂
	Layer thickness, nm	280	1220	800
	Top-down conductor area, cm ²		0.25	
2	Layer composition	Si@O@Al	LiPON	Li _x V ₂ O ₅
	Layer thickness, nm	180	1000	800
	Top-down conductor area, cm ²		0.25	
3	Layer composition	-	LiPON	LiCoO ₂
	Layer thickness, nm	0	1000	960
	Top-down conductor area, cm ²		0.25	

Charge and discharge curves were recorded in galvanostatic mode using multi-channel galvanostats/potentiostats P-20 × 8 and P-40× (Electrochemical Instruments, Chernogolovka, Russia). The results of measuring the specific capacity dependence on the charge current density for all three types of test cells are shown in Figure 1a. Figure 1 shows only discharge capacities because it turned out that charge capacity was very close to discharge capacity (the Coulombic efficiency was close to 100%). In Figure 1b, the same dependences are presented in bi-logarithmic coordinates to check the applicability of Peukert's equation (Equation (1)). Accordingly, the diagrams of cells 1 and 2 in Figure 1b Q(j) are well approximated by two linear segments, corresponding to two different Peukert's exponents values. For cell-1 (LiCoO₂), $\alpha'_1 = 0.33$ and $\alpha''_1 = 1.33$, and for cell-2 (Li_xV₂O₅), $\alpha'_2 = 0.21$ and $\alpha''_2 = 1.11$. In contrast, the Q(j) diagram of the anode-free cell can be fitted by a single linear segment with $\alpha_3 = 0.78$.

**Figure 1.** (a) Plots of discharge capacity versus charge current density Q(j) of test cells. Cells' electrochemical systems are shown in the inset. (b) The same dependences on a bi-logarithmic scale.

3. Anode Charging Model

To derive an equation modeling the dependence of capacity on current, an expression that relates the battery capacity to the lithium concentration at the anode–electrolyte

interface is needed. This expression can be derived from the simplified SSLIB model shown in Figure 2. The figure illustrates the distribution of lithium atoms in the anode and in the electrolyte. Conventionally, it is considered that the reduction in lithium ions occurs inside the δ -layer at the anode–electrolyte interface. This allows for formulating the boundary condition at the interface, which raises a question on the kind of boundary condition. Should it be condition of the 1st kind (Dirichlet condition) or 2nd kind (Neumann condition)? According to the explanation of the well-known Gibbs paradox [19,20], lithium ions and atoms are different particles that can form two opposite diffusion flows. Thus, the atomic δ -layer will diffuse into the anode, charging the latter, and into the electrolyte, creating a leakage current. In this case, one should equate the density of lithium sources in the δ -layer to the flows at the boundary, i.e., to choose the Neumann condition. It is this version of the boundary condition that was considered in the preprint of the present paper. However, the Neumann condition means that the lithium flow into the anode, hence its maximum charge, is proportional to the magnitude of the charging current, which contradicts the experimental results and Peukert’s law. Finally, this condition implies a large leakage current, which is inconsistent with the high value of the Coulomb efficiency.

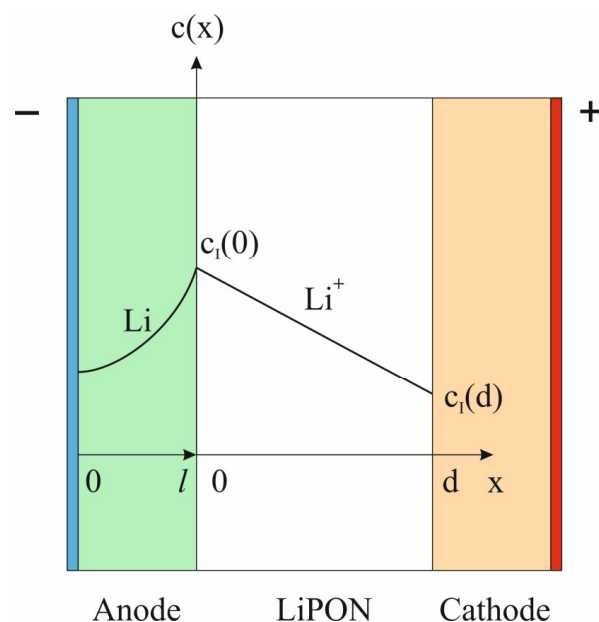


Figure 2. Stationary distribution of lithium ion concentration in the electrolyte and the instant distribution of lithium atoms in the anode.

At first glance, the Dirichlet condition also leads to contradictions. It means that the lithium particles in the anode near the interface and in the electrolyte are identical, i.e., these are lithium ions. But this can be explained by the fact that at low currents (i.e., at a high lithium concentration at the interface), only part of the ions is reduced directly in the boundary layer. This is because the reduction rate is determined by the current in the external circuit, which is small. The main mass of lithium diffuses into the anode, remaining in an ionized state and gradually reducing over time. In this case, the charge time is determined not by the rate of diffusion, but by the rate of lithium reduction already intercalated into the anode. It should be emphasized that the process of lithium intercalation is of a diffusion nature, since the field in the anode is shielded by a double electrical layer at the interface.

By virtue of the above arguments, when setting the boundary value problem for diffusion, the Dirichlet boundary condition $c(\ell, t) = c_l(0, \tau)$ was used, where $c(x, t)$ is the lithium concentration in the anode, ℓ is the interface coordinate, $c_l(0, \tau)$ is the lithium ion concentration at the electrolyte side of the interface, and τ is the so-called “slow time”. The latter implies that the concentration of lithium ions at the anode may slowly change during

charging. Then, the boundary value problem on lithium diffusion into the anode can be formulated as follows:

$$\begin{aligned}\frac{\partial}{\partial t}c(x, t) &= D \frac{\partial^2}{\partial x^2}c(x, t); \\ \left.\frac{\partial}{\partial x}c(x, t)\right|_{x=0} &= 0; \\ c(\ell, t) &= c_I(0, \tau); \\ c(x, 0) &= 0,\end{aligned}\tag{2}$$

where D is the diffusion coefficient of lithium.

The solution of boundary value problem (2) is sought by the Fourier method as

$$c(x, t) = c_I(0, \tau) - V(x)e^{-\mu^2 t}\tag{3}$$

Substituting the desired solution (3) into (2) results in the Sturm–Liouville problem:

$$\begin{aligned}\frac{\partial^2}{\partial x^2}V(x) + \frac{\mu^2}{D}V(x) &= 0; \\ \left.\frac{\partial}{\partial x}V(x)\right|_{x=0} &= 0; \\ V(x) &= 0; \\ V(x) &= c_I(0, \tau).\end{aligned}\tag{4}$$

Its solution is a sum of partial solutions:

$$V(x) = \sum_{n=0}^{\infty} C_n \cos\left(k_n \frac{x}{\ell}\right),\tag{5}$$

where $k_n = (2n + 1)\pi/2$. Substituting (5) into (3) gives the final form of the solution to boundary value problem (2):

$$c(x, t) = c_I(0, \tau) \left[1 - \sum_{n=0}^{\infty} (-1)^n \frac{2}{k_n} \cos\left(k_n \frac{x}{\ell}\right) e^{-k_n^2 \frac{D}{\ell^2} t} \right].\tag{6}$$

Equation (6) allows for finding the time-dependence of the anode charge as

$$Q(t) = qS\ell c_I(d) \left(1 - \sum_{n=0}^{\infty} \frac{2}{k_n^2} e^{-k_n^2 \frac{D}{\ell^2} t} \right) \rho(\tau),\tag{7}$$

where S is battery area, $\rho = c_I(0, \tau)/c_I(d)$, and $c_I(d)$ is the ion concentration at the cathode (Figure 2). An example of a charging curve is shown in Figure 3.

As follows from Figure 3a, the anode charging time does not exceed 150 s. The total specific charge $47.8 \mu\text{A} \cdot \text{h}/\text{cm}^2$ corresponds to the charge of cell-1 (LiCoO_2 cathode) at current density $24 \mu\text{A}/\text{cm}^2$. Hence, the time of lithium ion reduction is 1.99 h. At high current densities, the charging time, on the contrary, is determined by the diffusion process. For example, at $Q = 4.04 \mu\text{A} \cdot \text{h}/\text{cm}^2$ and $j = 960 \mu\text{A}/\text{cm}^2$ (Figure 3b), the charging time 15.2 s is an order of magnitude less than the time required for diffusion equalization of concentrations at the anode–electrolyte interface. An increase in the Peukert exponent, starting from a certain current density, may be due to the fact that the lithium concentration at the anode–electrolyte interface does not have time to reach the equilibrium value $c(0, \tau)$. An argument in favor of this assumption is the fact that the Peukert exponent for anode-free SSLIBs remains constant over the entire current range.

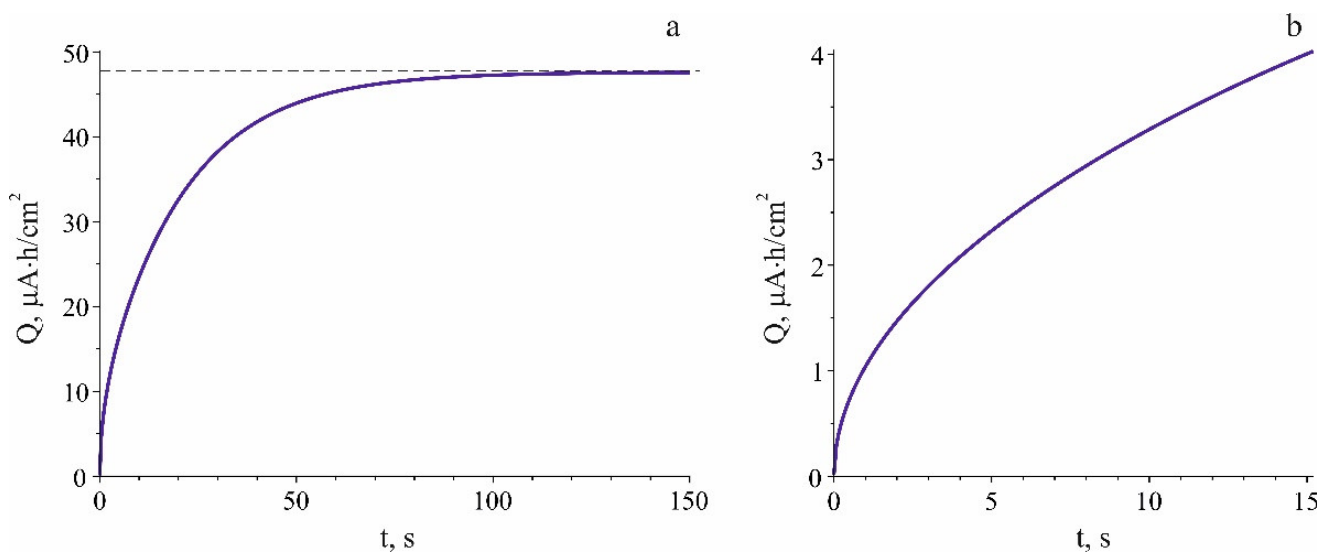


Figure 3. Charging curves according to Equation (7). **(a)** $Q(j)$ in a low-current area. Equation (7) parameters $\rho = 15c_l(d) = 2.55 \cdot 10^{27} \text{ m}^{-3}$; $\ell = 2.8 \cdot 10^{-7} \text{ m}$; $D = 1.5 \cdot 10^{-15} \text{ m}^2 \cdot \text{s}^{-1}$ correspond to maximum full charge $47.8 \mu\text{A} \cdot \text{h}/\text{cm}^2$ of cell-1 at current density of $24 \mu\text{A}/\text{cm}^2$. **(b)** High-current area. Equation (7) parameters $\rho = 2.1c_l(d) = 2.55 \cdot 10^{27} \text{ m}^{-3}$; $\ell = 2.8 \cdot 10^{-7} \text{ m}$; $D = 1.5 \cdot 10^{-15} \text{ m}^2 \cdot \text{s}^{-1}$ correspond to maximum full charge $4.04 \mu\text{A} \cdot \text{h}/\text{cm}^2$ at current density of $960 \mu\text{A}/\text{cm}^2$.

4. Dependence of the Lithium Concentration at the Anode–Electrolyte Interface on the Charge Current Density

Since the transport of lithium ions through the electrolyte is considered below and all the following equations refer to the segment $[0, d]$ in Figure 2, the notation $c(0)$ instead of $c_l(\ell)$ is used. The ion concentration at the anode–electrolyte interface $c(0)$ can be obtained from the balance condition for the electron current through the anode and the diffusion-drift current through the electrolyte. The total current density through the electrolyte is the sum of the drift and diffusion currents:

$$j_{DD}^E = \sigma_E \frac{U}{\varepsilon d} + q D_E \frac{dc(x)}{dx}, \quad (8)$$

where σ_E is the ionic conductivity of the electrolyte, U is the potential difference across the electrolyte layer, ε is the permittivity of the electrolyte, d is the thickness of the electrolyte layer, q is the lithium ion charge, D_E is the diffusion coefficient of the lithium ion in the electrolyte, and $c(x)$ is the concentration of lithium ions. Considering the relations $\sigma_E = \mu \bar{c} q$ and $D_E = \mu k_B T / q$, expression (8) can be written in the form

$$j_{DD}^{EI} = \mu q \frac{U \bar{c}}{\varepsilon d} + \mu k_B T \frac{dc}{dx}. \quad (9)$$

Within the framework of a simplified model, the concentration gradient can be considered linear:

$$\frac{dc}{dx} \approx \frac{c(d) - c(0)}{d}, \quad (10)$$

while concentration \bar{c} can be set equal to the average value of the concentration in the electrolyte $\bar{c} = [c(0) + c(d)]/2$. Then, the current density through electrolyte (9) takes the form

$$j_{DD}^{EI} = \frac{\mu}{d} k_B T c(d) \left[\left(\frac{qU}{2\varepsilon k_B T} - 1 \right) \rho + \left(\frac{qU}{2\varepsilon k_B T} + 1 \right) \right], \quad (11)$$

where $\rho = c(0)/c(d)$ is the ratio of the lithium ion concentrations at points 0 and d. This ratio can be expressed from Equation (11) as

$$\rho = \frac{j_{DD}^{El} d / \mu k_B T c(d) - (qU / 2\epsilon k_B T + 1)}{qU / 2\epsilon k_B T - 1}. \quad (12)$$

On the other hand, the current density (11) must be equal to the density of the electron current through the anode:

$$j_{DD}^{El} = \frac{U_p - U}{SR}, \quad (13)$$

where U_p is the voltage of the potentiostat output. Expressing U from (13) and its substitution into (12) yields

$$\rho = \frac{dj_{DD}^{El} / \mu k_B T c(d) - q(U_p - j_{DD}^{El} SR) / 2\epsilon k_B T - 1}{q(U_p - j_{DD}^{El} SR) / 2\epsilon k_B T - 1}. \quad (14)$$

Thus, relations (14) and (7) set up the dependence of the full charge on the charging current:

$$Q(j_{DD}^{El}) = Q_0 \cdot \frac{dj_{DD}^{El} / \mu k_B T c(d) - q(U_p - j_{DD}^{El} SR) / 2\epsilon k_B T - 1}{q(U_p - j_{DD}^{El} SR) / 2\epsilon k_B T - 1}, \quad (15)$$

where

$$Q_0 = qS\ell c_I(d). \quad (16)$$

The experimental (Figure 1) and theoretical (14) capacity dependences on the current density are compared in Figures 4 and 5, respectively.

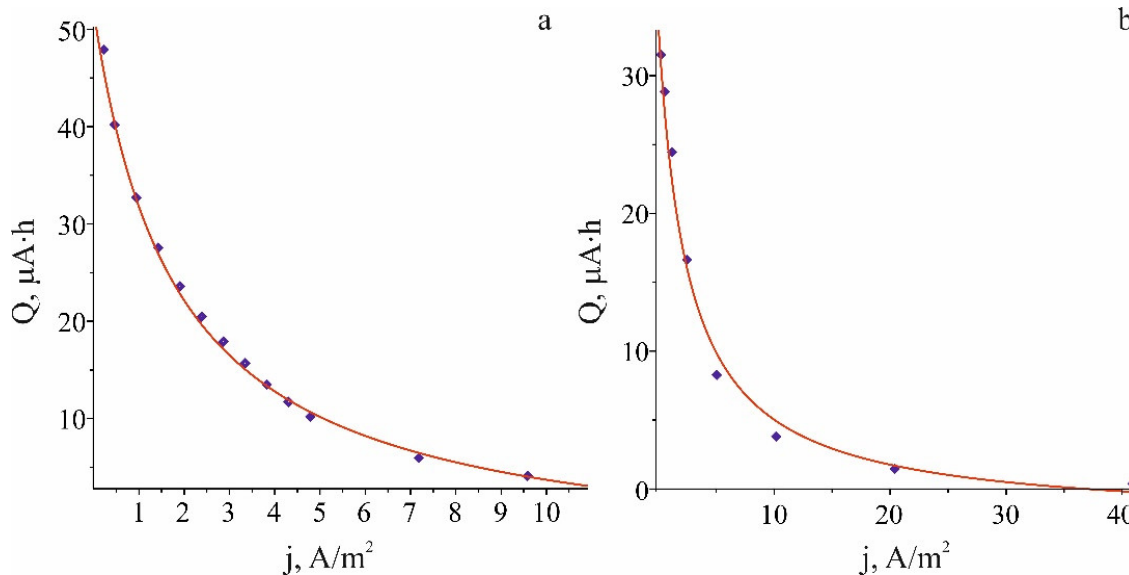


Figure 4. The theoretical (line) and experimental (diamonds) dependences of capacity on current density. (a) Experimental data on cell-1 and Equation (14) plotted with fitting parameters $c(d) = 2.55 \cdot 10^{27} \text{ m}^{-3}$; $\mu = 3 \cdot 10^{-12} \text{ m}^2 \text{ V}^{-1} \text{ s}^{-1}$; $d = 1.22 \cdot 10^{-6} \text{ m}$; $\ell = 280 \cdot 10^{-9} \text{ m}$; $T = 300 \text{ K}$; $\epsilon = 83$; $U_p = 3.8 \text{ V}$; $R = 2.7 \text{ k}\Omega$; $S = 10^{-4} \text{ m}^2$. (b) Experimental data on cell-2 and Equation (14) plotted with fitting parameters $c(d) = 2.2 \cdot 10^{27} \text{ m}^{-3}$; $\mu = 8.5 \cdot 10^{-12} \text{ m}^2 \text{ V}^{-1} \text{ s}^{-1}$; $d = 1.0 \cdot 10^{-6} \text{ m}$; $\ell = 180 \cdot 10^{-9} \text{ m}$; $T = 300 \text{ K}$; $\epsilon = 75$; $U_p = 3.5 \text{ V}$; $R = 1.5 \text{ k}\Omega$; $S = 10^{-4} \text{ m}^2$.

Judging by the shape of graphs in Figures 4 and 5, it is difficult to determine to what extent the experimental and theoretical dependences correspond to Peukert's law. Therefore, it is easier to show that the Peukert equation (Equation (1)) is a special case

of Equation (14), which takes place under the condition $qU_p/2\epsilon k_B T \approx 1$. In this case, Equation (14) takes the form

$$\rho \approx \frac{A}{j_{DD}^{EI}} - \left(1 + 2\epsilon \frac{\sigma_{An}d}{\sigma_{El}\ell} \right), \quad (17)$$

where $A = 2U_p/SR$, and σ_{An} and σ_{El} are the anode and the electrolyte conductivities, respectively. In its general form, Equation (14) describes the $Q(j)$ dependence more correctly, since, unlike (1), it does not suffer a singularity at the point $j = 0$ and imposes a limitation on current density.

The correspondence of the experimental and theoretical curves $Q(j)$ to Peukert's law is illustrated by Figure 6. It shows the results on the fitting of the experimental dependences by Equation (15) and the Peukert equation. The latter is presented in the form

$$Q(j) = \frac{A}{B + j^\alpha} - C, \quad (18)$$

where B and C are constants, imposing physical limits on capacity and current density. The Peukert exponent α and constants A , B , and C were used as fitting parameters, whose values are given in the caption to the figure. As can be seen from Figure 6, the differences between the graphs of Equations (15) and (18) are insignificant. Thus, it can be concluded that SSLIBs obey Peukert's law and that Equation (15) adequately approximates the experimental dependence $Q(j)$.

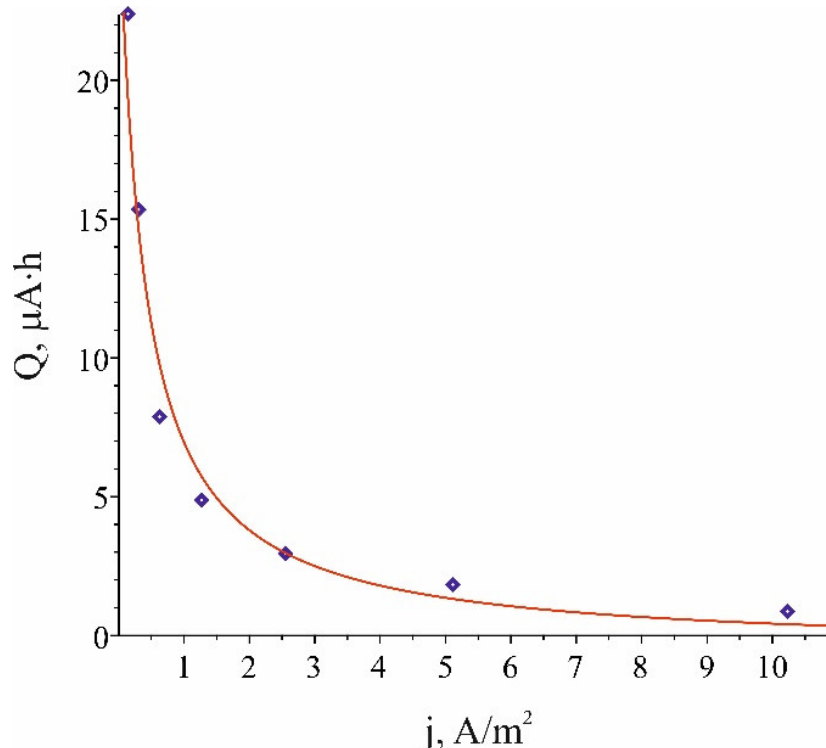


Figure 5. Anode-free cell. Experimental (diamonds) and theoretical (line) capacity dependences on current density. Fitting parameters $c(d) = 1.3 \cdot 10^{27} \text{ m}^{-3}$; $\mu = 8.5 \cdot 10^{-12} \text{ m}^2 \text{ V}^{-1} \text{ s}^{-1}$; $d = 1.0 \cdot 10^{-6} \text{ m}$; $\ell = 80 \cdot 10^{-9} \text{ m}$; $T = 300 \text{ K}$; $\epsilon = 80$; $U_p = 4.0 \text{ V}$; $R = 3.7 \text{ k}\Omega$; $S = 10^{-4} \text{ m}^2$.

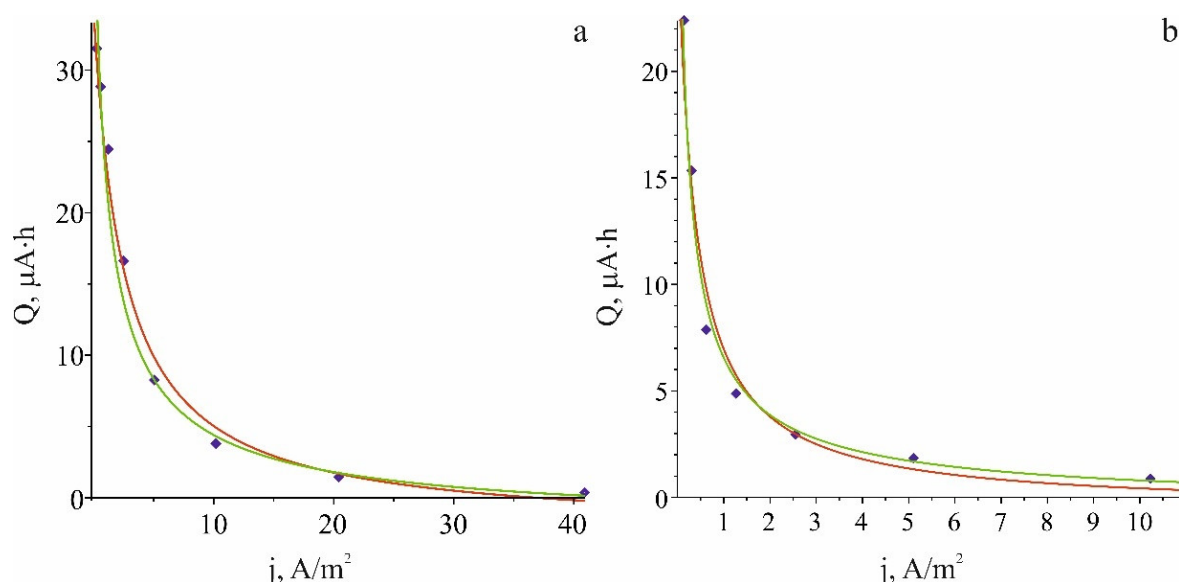


Figure 6. Experimental (diamonds) and theoretical (lines) dependences $Q(j)$ of cell-2 (a) and cell-3 (b). Red curve in panel (a) depicts dependence (15) with parameters $c(d) = 2.2 \cdot 10^{27}$; $\mu = 8.5 \cdot 10^{-12} \text{ m}^2 \text{ V}^{-1} \text{ s}^{-1}$; $d = 1.0 \cdot 10^{-6} \text{ m}$; $\ell = 180 \cdot 10^{-9} \text{ m}$; $T = 300 \text{ K}$; $\varepsilon = 75$; $U_p = 3.5 \text{ V}$; $R = 1.5 \text{ k}\Omega$; $S = 10^{-4} \text{ m}^2$. Green curve is a plot of Equation (18) with parameters $A = 28.15$; $B = 1$; $C = 1.2$; $\alpha = 0.82$. Red curve in panel (b) is Equation (15) plotted with parameters $c(d) = 1.3 \cdot 10^{27}$; $\mu = 8.5 \cdot 10^{-12} \text{ m}^2 \text{ V}^{-1} \text{ s}^{-1}$; $d = 1.0 \cdot 10^{-6} \text{ m}$; $\ell = 80 \cdot 10^{-9} \text{ m}$; $T = 300 \text{ K}$; $\varepsilon = 80$; $U_p = 4.0 \text{ V}$; $R = 3.7 \text{ k}\Omega$; $S = 10^{-4} \text{ m}^2$. Green curve depicts Equation (18) with parameters $A = 18.15$; $B = 0.18$; $C = 1.2$; $\alpha = 0.78$.

5. Summary

The example of SSLIBs of three different electrochemical systems shows that the capacity dependence on the density of the charging current (Figure 1) obeys Peukert's law. On the experimental curves $Q(j)$ of cell-1 and cell-2 (positive electrodes LiCoO_2 and $\text{Li}_x\text{V}_2\text{O}_5$) in bi-logarithmic coordinates, two sections with different slopes are clearly visible. These areas correspond to the Peukert exponent; $\alpha'_1 = 0.33$ and $\alpha''_1 = 1.33$ for cell-1; and $\alpha'_2 = 0.21$ and $\alpha''_2 = 1.11$ for cell-2. The $Q(j)$ graph of an anode-free cell has the form of an inclined straight line, which corresponds to the Peukert exponent $\alpha_3 = 0.78$.

To explain the reasons for the decrease in SSLIB capacity, the boundary value problem on lithium diffusion through the anode–electrolyte interface under a quasi-stationary boundary condition is considered. The substantiation of the choice of the first kind of boundary condition for the anode–electrolyte interface is given. Under this condition, the total charge of the anode is determined by the lithium ion concentration at the boundary. The relation between ion concentration at the anode interface and the total current density is obtained from the balance condition for diffusional, drift, and total currents. It is shown that the concentration of ions at the anode–electrolyte interface, and, accordingly, the total charge of the battery are described by the expression $Q(j)$ similar to Peukert's law.

The resulting expression more correctly describes the dependence $Q(j)$, in the sense that it considers the limited capacity of the battery and current density. A comparison of the experimental curves and the results of their approximation by the theoretical dependence $Q(j)$ and Peukert's law shows that the experimental points fit well enough on the approximating curves. From this result, two conclusions can be drawn: (i) solid-state thin-film lithium-ion batteries obey Peukert's law; (ii) the resulting dependence $Q(j)$ can be considered as a simplified battery model consistent with Peukert's empirical law.

Although the experimentally observed changes in the Peukert exponent do not directly follow from the obtained relationships, the latter allow us to make some assumptions about the causes of these changes. The essence of these assumptions is as follows. Within the

framework of the model, the processes of lithium diffusion into the anode and the reduction in lithium ions in the anode proceed independently of each other. At a low current density, the diffusion rate of lithium ions exceeds the rate of their reduction, as a result of which the lithium concentration in the anode is set equal to its concentration at the boundary. The charging time in this case is determined by the reduction time of lithium ions.

In the process of setting a stationary concentration distribution in the electrolyte, a large contribution to the total current falls on the displacement current j_D . After the steady state is established, the displacement current decays, and the total current j_{tot} is determined only by the rate of lithium ion reduction in the anode G_{red} . Up to some j_{tot} value, the reduction rate does not depend on the ion concentration at the anode boundary. At a certain j_{tot} value, the reduction rate G_{red} and the diffusion current of ions through the boundary are equalized, i.e., the total current reaches saturation $j_{tot} = j_s$. From this point on, the rate of ion reduction depends on their concentration at the boundary $G_{red}(\rho)$. Charging the battery under the condition $j_{tot} \geq j_s$ is still possible, but its time is limited by the time during which the condition $j_D + G_{red} \geq j_{tot}$ is held. When the displacement current decreases and meets the condition $j_D + G_{red} < j_{tot}$, the potentiostat is no longer able to maintain the set current, which leads to an increase in the output voltage.

We believe that the current at which the increase in the Peukert exponent begins corresponds to the saturation current, determined by the reduction rate of lithium ions $j_{tot} = G_{red}$. With a further increase in the total current, there is a simultaneous decrease in the rate of ion reduction $G_{red}(\rho)$, since their concentration at the interface decreases, and a decrease in the charge time, determined by the condition $j_D + G_{red} \geq j_{tot}$. Thus, the proposed model makes it possible to qualitatively explain the Peukert exponent's dependence on the charge current density.

Author Contributions: A.S.R.—conceptualization, writing of original draft; A.M.S.—supervision, methodology; A.A.M.—investigation; V.V.N.—investigation, visualization. All authors have read and agreed to the published version of the manuscript.

Funding: This research was funded by the Ministry of Science and Higher Education of the Russian Federation grant number 0856-2020-0006.

Data Availability Statement: Supporting reported results data can be found or obtained by demand at The Facilities Sharing Centre “Diagnostics of Micro- and Nanostructures” (FSC DMNS), P.G. Demidov Yaroslavl State University.

Conflicts of Interest: The authors declare that they have no conflicts of interest. The funders had no role in the design of the study; in the collection, analyses, or interpretation of data; in the writing of the manuscript, or in the decision to publish the results.

References

1. Skundin, A.; Kulova, T.; Rudy, A.; Mironenko, A. *All Solid State Thin-Film Lithium-Ion Batteries: Materials, Technology, and Diagnostics*, 1st ed.; CRC Press: Boca Raton, FL, USA; Taylor & Francis Group: Boca Raton, FL, USA, 2021; 214p, ISBN 9780367086824.
2. Sun, C.; Liu, J.; Gong, Y.; Wilkinson, D.P.; Zhang, J. Recent advances in all-solid-state rechargeable lithium batteries. *Nano Energy* **2017**, *33*, 363–386. [[CrossRef](#)]
3. Patil, A.; Patil, V.; Shin, D.W.; Choi, J.-W.; Paik, D.-S.; Yoon, S.-J. Issue and challenges facing rechargeable thin film lithium batteries. *Mat. Res. Bull.* **2008**, *43*, 1913–1942. [[CrossRef](#)]
4. Ferrari, S.; Loveridge, M.; Beattie, S.D.; Jahn, M.; Dashwood, R.J.; Bhagat, R. Latest advances in the manufacturing of 3D rechargeable lithium microbatteries. *J. Power Sources* **2015**, *286*, 25–46. [[CrossRef](#)]
5. Yu, X.; Bates, J.B., Jr.; Hart, G.E.J.; Hart, F.X. A Stable Thin-Film Electrolyte: Lithium Phosphorus Oxynitride. *J. Electrochem. Soc.* **1997**, *144*, 524–532. [[CrossRef](#)]
6. Yi, X.; Feng, Y.; Rao, A.; Zhou, J.; Wang, C.; Lu, B. Quasi-Solid Aqueous Electrolytes for Low-Cost Sustainable Alkali-Metal Batteries. *Adv. Mater.* **2023**, e202302280. [[CrossRef](#)] [[PubMed](#)]
7. Rudy, A.S.; Mironenko, A.A.; Naumov, V.V.; Fedorov, I.S.; Skundin, A.M.; Tortseva, Y.S. Thin-Film Solid State Lithium-Ion Batteries of the LiCoO₂/Lipon/Si@O@Al System. *Russ. Microelectron.* **2021**, *50*, 333–338. [[CrossRef](#)]
8. Rudy, A.S.; Kurbatov, S.V.; Mironenko, A.A.; Naumov, V.V.; Skundin, A.M.; Egorova, Y.S. Effect of Si-Based Anode Lithiation on Charging Characteristics of All-Solid-State Lithium-Ion Battery. *Batteries* **2022**, *8*, 87. [[CrossRef](#)]

9. Peukert, W. Über die Abhängigkeit der Kapazität von der Entladestromstärke bei Bleiakkumulatoren. *Elektrotechnisch Z.* **1897**, *27*, 287–288. (In German)
10. Baert, D.; Vervaet, A. Lead-acid battery model for the derivation of Peukert's law. *Electrochim. Acta* **1999**, *44*, 3491–3504. [[CrossRef](#)]
11. Ekunde, P. A simplified model of the lead/acid battery. *J. Power Sources* **1993**, *46*, 251–262. [[CrossRef](#)]
12. Bouet, J.; Pompon, J.P. Analyse des causes de dégradation des plaques positives de batteries au plomb. *Electrochim. Acta* **1981**, *26*, 1477–1487. [[CrossRef](#)]
13. Doerffel, D.; Abu Sharkh, S. A critical review of using the Peukert equation for determining the remaining capacity of lead-acid and lithium-ion batteries. *J. Power Sources* **2006**, *155*, 395–400. [[CrossRef](#)]
14. Du, F.; Zhao, N.; Li, Y.; Chen, C.; Liu, Z.; Guo, X. All solid state lithium batteries based on lamellar garnet-type ceramic electrolytes. *J. Power Sources* **2015**, *300*, 24–28. [[CrossRef](#)]
15. Omar, N.; Bossche, P.V.d.; Coosemans, T.; Van Mierlo, J. Peukert Revisited—Critical Appraisal and Need for Modification for Lithium-Ion Batteries. *Energies* **2013**, *6*, 5625–5641. [[CrossRef](#)]
16. Bergveld, H.J.; Kruijt, W.S.; Notten, P.H.L. *Battery Management Systems: Design by Modelling*; Kluwer: Amsterdam, The Netherlands, 2002; Chapter 6, pp. 193–239.
17. Lerner, S.; Lennon, H.; Seiger, H.N. Development of an alkaline battery state of charge indicator. In *Power Sources*; Collins, D.H., Ed.; Oriel Press: Newcastle, UK, 1970; pp. 135–137.
18. Wu, G.; Lu, R.; Zhu, C.; Chan, C.C. An Improved Ampere-Hour Method for Battery State of Charge Estimation Based on Temperature, Coulomb Efficiency Model and Capacity Loss Model. In Proceedings of the IEEE Vehicle Power and Propulsion Conference (VPPC), Lille, France, 1–3 September 2010; pp. 1–4.
19. Wiedeburg, O. Das Gibbs'sche Paradoxon. *Ann. Phys.* **1894**, *289*, 684–697. [[CrossRef](#)]
20. Jaynes, E.T. The Gibbs paradox. In *Maximum Entropy and Bayesian Methods*; Smith, C.R., Erickson, G.J., Neudorfer, P.O., Eds.; Kluwer Academic Publishers: Dordrecht, The Netherlands, 1992; pp. 1–22.

Disclaimer/Publisher's Note: The statements, opinions and data contained in all publications are solely those of the individual author(s) and contributor(s) and not of MDPI and/or the editor(s). MDPI and/or the editor(s) disclaim responsibility for any injury to people or property resulting from any ideas, methods, instructions or products referred to in the content.